



CHALMERS
UNIVERSITY OF TECHNOLOGY

One stone two birds: conjugation of graphene oxide with Rg3–doxorubicin reduces its toxicity and downregulates metallothionein expression for

Downloaded from: <https://research.chalmers.se>, 2026-04-14 03:36 UTC

Citation for the original published paper (version of record):

Balusamy, S., Rahimi, S., Tkachova, O. et al (2025). One stone two birds: conjugation of graphene oxide with Rg3–doxorubicin reduces its toxicity and downregulates metallothionein expression for improved liver-targeted therapy. *Cancer Nanotechnology*, 16(1). <http://dx.doi.org/10.1186/s12645-025-00345-y>

N.B. When citing this work, cite the original published paper.

RESEARCH

Open Access



One stone two birds: conjugation of graphene oxide with Rg3–doxorubicin reduces its toxicity and downregulates metallothionein expression for improved liver-targeted therapy

Sri Renukadevi Balusamy¹, Shadi Rahimi^{2†}, Olena Tkachova², Seungah Lee³, Suresh Ramakrishna^{4,5}, Ivan Mijakovic^{2,6*} and Haribalan Perumalsamy^{7,8*}

[†]Sri Renukadevi Balusamy and Shadi Rahimi have contributed equally and are co-first authors.

*Correspondence: ivan.mijakovic@chalmers.se; harijai2004@gmail.com

² Systems and Synthetic Biology Division, Department of Life Sciences, Chalmers University of Technology, SE-412 96 Gothenburg, Sweden
⁷ Research Institute for Convergence of Basic Science, Hanyang University, Seoul 04763, South Korea
Full list of author information is available at the end of the article

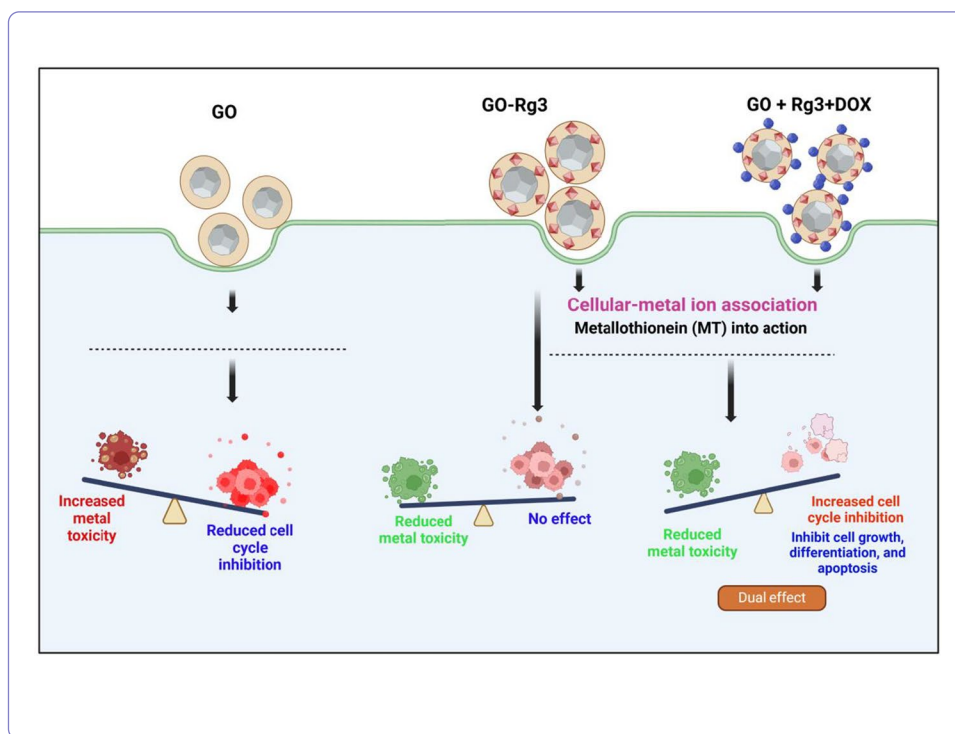
Abstract

Although the role of metallothionein (MT) in various cancers has been extensively studied, its expression upon treatment with the ginsenoside Rg3 and doxorubicin-coated graphene-based nanoparticles (GO–Rg3–DOX) has not yet been elucidated. Using RNA sequencing, we elucidated how GO–Rg3–DOX arrested cell growth by modulating Wnt signaling and the cell cycle pathway. For this purpose, RNA-seq datasets of graphene oxide (GO), GO–Rg3, and GO–Rg3–DOX were used to explore the expression of MT genes and cell growth-dependent pathways in Huh7 cells, a human liver cancer cell line. Our analysis revealed that the MT gene family plays a major role in the induction of oxidative stress in Huh7 cells. In particular, cell–metal association triggered oxidative stress in the GO-treated group via MT gene downregulation, upregulation of the extracellular matrix–receptor interaction pathway, and downregulation of the Wnt signaling pathway and oxidative phosphorylation, resulting in cancer cell growth inhibition. In contrast, the GO–Rg3 combination group showed an upregulation of MT genes, indicating reduced toxicity and oxidative stress upon Rg3 conjugation. Finally, the GO–Rg3–DOX complex exhibited significant cellular association with minimal toxicity in Huh7 cells, leading to the downregulation of Wnt signaling and cell cycle pathways. Overall, our study clearly demonstrates that the GO–Rg3–DOX complex has significant anticancer therapeutic potential, which warrants further *in vivo* studies.

Keywords: Liver cancer, GO–Rg3–DOX, GO–Rg3, Cell cycle, Metallothionein

Graphical abstract





Introduction

Graphene oxide (GO) is an attractive nanocarrier with high loading capacity for anticancer drugs. GO also plays a significant role in other applications, including biosensing/bioimaging, nano-detecting, gene/drug delivery, tissue engineering, and regenerative medicine (Guo et al. 2011; Si and Lang 2018; Wang et al. 2012; Yang et al. 2011). However, the cellular absorption mechanisms for GO can potentially trigger GO-induced toxicity to liver cells (HepG2, Huh7) and macrophages (Lammel et al. 2013; Li et al. 2012; Rahimi et al. 2023; Rahimi et al. 2022). GO can supply electrons to electron transport chain complexes I and II by acting as an electron donor to induce reactive oxygen species (ROS) mediated cytotoxicity. Moreover, GO can also modulate genes involved in oxidative phosphorylation, which perturbs mitochondrial functioning. Our previous study demonstrated GO induces ROS-mediated cytotoxicity through the reduced expression of glutathione biosynthesis genes and decreased ROS scavengers. Moreover, GO targets overexpressing genes involved in the IL-6/JAK/STAT3 pathway that plays a crucial role in the growth and development of several cancers (Johnson et al. 2018; Rahimi et al. 2023). Another report demonstrated that GO at lower doses administered to prostate cancer (PC3) cells induced proliferation by activation of the PI3K/AKT/mTOR and TGF- β signaling pathways (Zhu et al. 2020). As a result, GO alone is considered more detrimental, despite its commendable biological features. Therefore, developing alternate approaches that minimize GO-induced toxicity can help to ensure their long-term use.

Functionalization of graphene nanomaterials with biocompatible molecules alters the physicochemical properties of GO, resulting in lower cytotoxicity and better biocompatibility both in vitro and in vivo (Jiang et al. 2021; Qu et al. 2018; Zhang et al. 2017). The

ginsenoside Rg3 is a major ginsenoside known for its significant therapeutic effects in various liver diseases, including hepatocellular carcinoma (HCC), through the activation of various cell death mechanisms, such as apoptosis and autophagy, which involve regulatory inputs of multiple signaling pathways. Rg3 is also known to inhibit cancer cell proliferation by suppressing angiogenesis and migration, including HCC cells. Despite the tremendous advantages of Rg3, its applications are limited because of its low molecular weight, poor solubility, and limited bioavailability (Wang et al. 2024).

Metallothionein (MT) is a cysteine-rich protein considered a potent antioxidant due to its high sulfhydryl content, which can effectively scavenge free radicals and prevent oxidative damage to cells, thus being involved in metal detoxification (Roesijadi 1996; Yang et al. 2024). The MT family contains 11 active genes in humans, which are divided into four classes, M1, M2, M3, and M4; M1 and M2 are expressed in various organs and tissues, MT3 is mainly expressed in the brain, and MT4 is expressed in squamous epithelial cells (Moffatt and Séguin 1998; Sutherland and Stillman 2014). They bind to metal ions and protect cells from metal-induced toxicity by maintaining cellular homeostasis. However, MT gene expression largely varies depending on the cancer cell type, and its regulation contributes to protection against DNA damage and apoptosis. MTs are also involved in tumor growth, cancer cell progression, metastasis, and drug resistance. For instance, MT genes are highly expressed in breast, ovarian, nasopharyngeal, urinary bladder, and melanoma cancers and are often downregulated in prostate and papillary thyroid carcinomas (Si and Lang 2018; Yang et al. 2024). Their expression varies even among lung cancer cell types. For example, MT expression is observed in squamous cell carcinoma of the lung and adenocarcinoma, but not in small cell lung cancer (Si and Lang 2018). Thus, a better understanding of MT expressions in various cancers will aid in identifying specific targets and effectively treating cancer. Therefore, our study aimed to understand the role of MT genes in GO–Rg3–DOX treatment of hepatocarcinoma cells and how GO–Rg3–DOX inhibits the growth of cancer cells while inducing cell cycle arrest and obstructing the Wnt signaling pathway. To accomplish this, we used RNA sequencing (RNA-seq) and subsequently validated the data using quantitative PCR (qPCR).

Material and methods

Preparation of GO–Rg3 and GO–Rg3–DOX

Ultra-highly concentrated single-layer GO was bought from the Graphene Supermarket. GO–Rg3 was synthesized by esterifying GO and Rg3 in the presence of concentrated sulfuric acid, and GO–Rg3–DOX was synthesized by mixing GO–Rg3 with DOX overnight at pH 8 (Fig. 1) (Rahimi et al. 2023).

Sample information

Human Huh7 hepatoma cells were grown at 37 °C and 5% CO₂ in Dulbecco's Modified Eagle's Medium containing 4500 mg L⁻¹ glucose, further supplemented with 10% fetal bovine serum, 100 U mL⁻¹ of penicillin, and 100 µg mL⁻¹ of streptomycin. The cells were treated with (i) GO, (ii) GO–Rg3, and (iii) GO–Rg3–DOX (Rahimi et al. 2023).

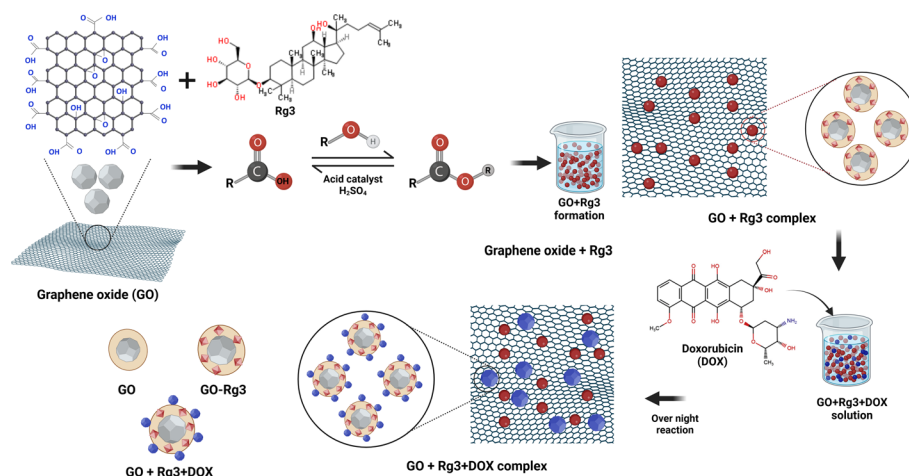


Fig. 1 Schematic representation of synthesis of GO-based nanoparticles

Dataset information

Previously, our original RNA-seq datasets were uploaded to the NCBI GEO database and received the accession number GSE185139. In this study, we downloaded our own datasets and reanalyzed them for a deeper understanding of cellular–metal associations and their transcriptomic responses. The datasets consisted of more than 12 samples grouped as GO alone, GO–Rg3, GO–Rg3–DOX, or untreated. Each group had three replicate datasets of Huh7 cells.

Data processing

The unprocessed raw data from each group were processed to remove low-quality and unread information, and we discovered 317,556 genes in the 12 samples. The scatter plot of the GO versus control groups revealed good-quality reads, with a linear regression score of $R=0.980$. Similarly, the linear regression values for GO–Rg3 versus control and GO–Rg3–DOX versus control groups were 0.989 and 0.961, respectively (Fig. 2a). Principal component analysis (PCA) clearly demonstrated the percentage variance across groups and revealed substantial differences among the three groups (Fig. 2b).

Differentially expressed analysis

Differentially expressed analysis was performed for each group exposed to the GO, GO–Rg3, and GO–Rg3–DOX combinations compared to untreated groups. This revealed significant transcriptomic changes in each group, and differentially expressed genes (DEGs) were observed, which included both upregulated and downregulated genes. To distinguish between up- and down-regulated genes, we performed volcano plots by setting a \log_2 -fold change and p -value cut-off. Gene network analysis was performed using string network analysis (<https://string-db.org/>) to reveal interactions between genes and their associated molecular pathways.

Gene ontology enrichment analysis

For functional annotation studies, we performed gene ontology enrichment analysis, which included biochemical processes, cellular components, and molecular functions.

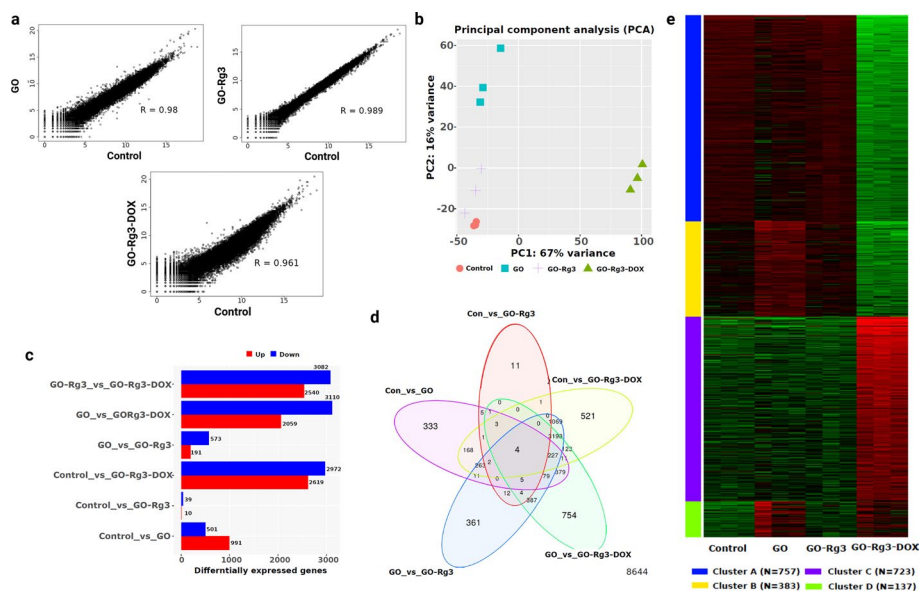


Fig. 2 Comparison of GO, GO-Rg3, and GO-Rg3-DOX treated groups. **a** Scatter plot of transformed expression of the three different groups compared to untreated control group. **b** Principal component analysis showed significant variance among the different groups. **c** Bar graph analysis showing comparison of differentially expressed genes (DEGs), up- and down-regulated from each group. **d** Venn diagram analysis revealed commonly shared as well as unique DEGs between different groups. **e** Heat map comparison of the GO-, GO-Rg3-, and GO-Rg3-DOX-treated groups compared to untreated control groups. DEGs were defined as an adjusted p -value (Benjamini-Hochberg analysis) of less than 0.05 and $|\log_2FC| > 2$

For the analysis, we used two different platforms, gProfiler (<https://biit.cs.ut.ee/gprofiler/gost>) and DAVID (<https://david.ncifcrf.gov/home.jsp>), to compare the best and well-defined annotation information. To identify significant DEGs from each sample group, both analytical tools listed important entities involved in biochemical processes, cellular components, and molecular functions. Based on the probable similarity score, p -value, gene counts, and false discovery rate (FDR) score, we shortlisted the most enriched terms to interpret the genes from each sample group involved in molecular function.

Gene set enrichment analysis

GSEA analysis (GSEA) was conducted (<https://www.gsea-msigdb.org/gsea/index.jsp>) for specific DEGs that significantly contributed to the determination of the molecular pathways involved. This method analyzes almost all genes from each cell type and its subsets without using a gene filtering threshold. The data were evaluated using the normalized enrichment score, which measures the enrichment of each pathway on the list. Positive and negative net values indicate enrichments at the top and bottom of the list, respectively.

Reverse transcription quantitative PCR

Cells were seeded onto 6-well plates at a density of 4×10^5 cells per well and cultured for 24 h before treatment with GO, GO-Rg3, GO-Rg3-DOX, and DOX for 6 h. Medium was used as the negative control. Three replicates were performed for each treatment. After treatment, the cells were washed three times with phosphate-buffered saline. Total RNA was extracted using the RNeasy Mini Kit (Qiagen, Hilden, Germany), and its

quality was examined using a Bioanalyzer (Agilent, Santa Clara, CA, USA) and an Agilent RNA 6000 Nano Kit (Rahimi et al. 2023). Specific reverse transcription qPCR primers were designed for these genes (Table S1). The beta actin gene was used as an internal reference. cDNA was synthesized from isolated RNA. Gene expression was analyzed using qPCR (Peng et al. 2010). The relative gene expression values were assessed using Agilent Technologies Stratagene Mx30005 P and calculated according to the manufacturer's instructions (Chen et al. 2005).

Statistical analysis

Genes differentially expressed were defined as an adjusted *p*-value (Benjamini–Hochberg analysis) of less than 0.05 and a fold change greater than twofold. In all gene ontology and GSEA experiments, an adjusted *p*-value (Benjamini–Hochberg analysis) of less than 0.05 was used to detect significant enrichment.

Results and discussion

GO–Rg3-treated cells show a similar pattern of gene expression as control cells

The ultra-concentrated, single-layer graphene oxide (GO) was procured from Graphene Supermarket. According to the supplier's specifications, the product contains over 80% single-layer GO with flake sizes ranging from 0.5 to 5 μm . To achieve uniform and consistent flake dimensions, the GO dispersion was subjected to probe sonication for 1.5 min. Post-sonication, the average GO lateral size was measured as 181.38 ± 2.2 nm, and the thickness was found to be 1–2 nm, as determined by atomic force microscopy (AFM). Upon conjugation with ginsenoside Rg3 and subsequent loading of doxorubicin (DOX), the flake size increased to 1.5–2 μm . The presence of DOX on the GO–Rg3 complex was visualized as nanoscale dots corresponding to increased height profiles on the GO surface, also confirmed by AFM. No sedimentation or turbidity change after hours/days at 4 °C and under mild shaking indicates physical stability.

To demonstrate the effect of Rg3 and DOX conjugated with GO on hepatocarcinoma cells, we performed gene expression analysis of Huh7 cells treated with GO, GO–Rg3, and GO–Rg3–DOX and compared them to the untreated control cells. A scatter plot of the transformed expression of the three different groups (GO, GO–Rg3, and GO–Rg3–DOX) compared to that of the untreated control group showed a linear relationship (Fig. 2a). The PCA demonstrated that the treatment and control samples could be distinctly classified (Fig. 2b). In addition, the GO–Rg3 treated samples exhibited a slight variance compared to the control samples (Fig. 2b), proving the biocompatibility of GO–Rg3 compared to GO alone. In the case of DEGs, only a few genes were differentially expressed (10 upregulated and 39 downregulated genes) following GO–Rg3 treatment compared to the control (Fig. 2c). The Venn diagram indicates that 11 genes were uniquely differentially expressed following GO–Rg3 treatment compared to the control (Fig. 2d). In contrast, 333 and 521 genes were uniquely differentially expressed by GO and GO–Rg3–DOX, respectively, compared with the control. The heat map of gene expression in the GO-, GO–Rg3-, and GO–Rg3–DOX-treated groups compared with the untreated control group displayed four gene clusters (A–D) (Fig. 2e). Interestingly, the heat maps of the control and GO–Rg3 groups showed similar patterns for all gene clusters.

MT2 is associated with a high Edmondson–Steiner grade, microvascular invasion, and poor prognosis (Park and Yu 2013). MT1 and MT2 double knockout accelerates hepatocarcinogenesis in mice exposed to the carcinogen diethylnitrosamine (Majumder et al. 2010).

In an attempt to identify prognostic biomarkers for predicting biochemical recurrence of prostate cancer, 455 DEGs were identified. MT1E downregulation is a potential biomarker of early biochemical recurrence and poor prognosis in patients with prostate cancer (Demidenko et al. 2017). MT1E enhances the migration and invasion of human glioma cells by inducing MMP-9 inactivation via the upregulation of NF- κ B p50 (Ryu et al. 2012). MT1E may function as a potent tumor suppressor in HCC, and its decreased expression leads to abnormal cell metastasis (Liu et al. 2020). Similarly, the expression of MT1F in HCC tissue correlated with growth suppression and exogenous MT1F showed a strong growth-inhibitory effect on HepG2 cells (Lu et al. 2003). Thus, our results on the downregulation of MT1F and MT1E (Fig. 3b) due to GO treatment may be correlated with the enhanced growth of Huh7 cells, which was previously reported by our group (Rahimi et al. 2023).

In addition to MTs, we found DEGs with biological functions in growth (FGF7, BDNF, PRKG1, DUOX2, ACVRL1, and KCNJ8) in the GO-treated group compared to the control. FGF7, BDNF, PRKG1, and KCNJ8 were downregulated, whereas DUOX2 and ACVRL1 were upregulated. Among these genes, FGF7, BDNF, and PRKG1 interact with each other.

Regarding the enrichment of gene sets, extracellular matrix (ECM)–receptor interaction, EGFR tyrosine kinase inhibitor resistance, and hypoxia-inducible factor-1 (HIF-1) signaling gene sets were enriched with positive enrichment scores, whereas oxidative phosphorylation, Wnt signaling, and ribosome-related gene sets were enriched with negative enrichment scores (Fig. S1b). The rapid proliferation of cancer cells leads to rapid consumption of tissue oxygen. Thus, the oxygen consumption rate exceeds the oxygen rate supplied by the circulation, leading to hypoxia (McKeown 2014). The hypoxic state results in a series of adaptive responses that are mainly mediated by HIFs. The human genome encodes three different HIF subtypes: HIF-1 α , HIF-2 α and HIF-3 α (Guo et al. 2020). In our study, the increased proliferation of Huh7 cells, along with HIF-1 signaling gene set enrichment, may be a potential indicator of hypoxia in GO-treated cells. Consistent with our results, Mukherjee et al. previously reported the angiogenic properties of GO (Mukherjee et al. 2015). They suggested that the intracellular formation of reactive oxygen species and reactive nitrogen species as well as the activation of phosphorylated endothelial nitric oxide NOS and Akt might be probable mechanisms for GO-induced angiogenesis (Mukherjee et al. 2015). The unwanted effects of GO carriers on cell proliferation and angiogenesis suggest limitations in using GO alone as a drug carrier for cancer treatment.

In addition to the unwanted effects of GO carriers on proliferation and angiogenesis, downregulation of oxidative phosphorylation genes was observed in the GO-treated group (Fig. S1b). This was consistent with the effect of GO on the downregulation of oxidative phosphorylation complex genes in glioblastoma (Szmids et al. 2019). Furthermore, Zhou et al. (2014) showed that polyethylene glycol-modified GO

significantly impaired mitochondrial oxidative phosphorylation in breast cancer cells but did not affect oxidative phosphorylation in non-cancerous cells (Zhou et al. 2014).

Conjugation of GO with Rg3 reduces its unwanted effects on growth and angiogenesis-related genes

To determine whether conjugation of Rg3 with GO could reduce the toxicity of GO, we performed RNA-seq analysis on control and GO–Rg3-treated Huh7 cells. The significantly downregulated (blue) and upregulated (red) genes are represented in a volcano plot (Fig. S2a). Among the 49 genes that were differentially expressed by GO–Rg3, 10 were upregulated and 39 were downregulated (Fig. S2d). The ECM–receptor interaction, JAK–STAT signaling pathway, and longevity-regulating pathway-related gene sets were positively enriched, whereas the oxidative regulation, proteasome, and ribosome-related gene sets were negatively enriched (Fig. S2f).

When we compared the heat map of gene expression in the GO–Rg3-treated group with that in the GO-treated group (Fig. 4), we found 191 upregulated and 573 downregulated genes (Fig. 4c). Cell cycle, basal transcription factors, and DNA replication gene sets were positively enriched, whereas cytokine–cytokine receptor interaction, Notch signaling pathway, and HIF-signaling pathway gene sets were negatively enriched in GO–Rg3 compared to those in GO (Fig. S3a). Gene ontology analysis (Biological Process) of the top DEGs revealed that genes with biological functions such as stress response to metal ions, detoxification of inorganic compounds, intracellular zinc ion homeostasis, response to copper ions, response to zinc ions, detoxification, response to

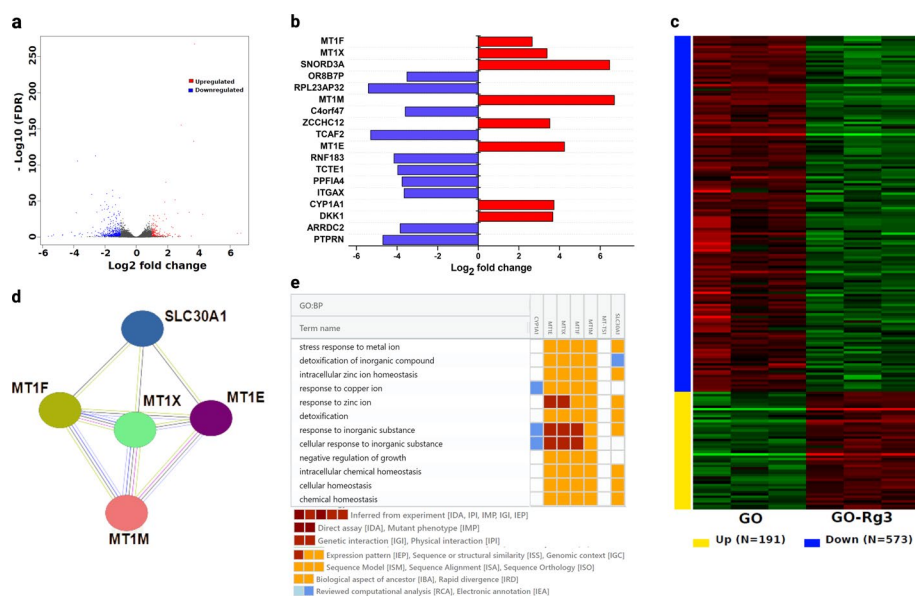


Fig. 4 Transcriptomic analysis comparing the GO and GO–Rg3 groups. **a** Volcano plot showing significant down (blue) and upregulated (red) DEGs. **b** Bar graph showing the \log_2 fold change values for significant DEGs that are highly expressed. **c** Heat map showing the total gene expression for the GO and GO–Rg3 groups. **d** Network analysis of metallothionein-associated genes interaction. **e** Analysis of biological processes for metallothionein-associated genes representing possible cellular metal association. DEGs were defined as an adjusted p -value (Benjamini–Hochberg analysis) of less than 0.05 and $|\log_2\text{FC}| > 2$. In gene ontology experiment, an adjusted p -value (Benjamini–Hochberg analysis) of less than 0.05 was used to detect significant enrichment

inorganic substances, cellular response to inorganic substances, negative regulation of growth, intracellular chemical homeostasis, cellular homeostasis, and chemical homeostasis were enriched (Fig. 4e). Interestingly, the MT genes, MT1F, MT1X, and MT1E, which were downregulated by GO, were upregulated by GO–Rg3 (Fig. 4b). We further validated the RNA-seq results for the MT genes using qPCR. GO induced the downregulation of MT genes compared to the control group (Fig. 5); however, there was no significant difference in the expression of MT genes, except for MT2A, between the GO–Rg3 and control groups. In fact, the MT genes were negatively regulated by GO treatment, whereas GO–Rg3 treatment had the opposite effect. The confirmation of MT protein-level could further strengthen our findings. As such, future studies will include targeted proteomic approaches (e.g., ELISA or LC–MS/MS) to validate specific MT isoform changes at the protein level.

As previously described by our group (Rahimi et al. 2023), GO–Rg3-treated Huh7 cells showed no significant difference in growth compared with untreated control cells. Thus, the upregulation of MTs, enrichment of the negative regulation of growth-related genes, and normal cell growth support the hypothesis that Rg3 conjugation mitigates GO toxicity. Another finding supporting this is that the HIF-1 gene set that was positively enriched by GO was negatively enriched by GO–Rg3. The antiangiogenic properties of Rg3 have been well studied (Cao et al. 2017; Nakhjavani et al. 2020; Tang et al. 2018; Yue et al. 2006). Rg3 prolonged the survival of an orthotopic HCC model by inducing apoptosis and inhibiting angiogenesis. In fact, Rg3 can initiate apoptotic progress in liver tumors, which is followed by the weakening of the tumor volume and capability to produce a vascularized network for further tumor growth and remote metastasis (Hu et al. 2019). Based on the results presented herein, GO–Rg3 can be considered a biocompatible drug carrier for cancer treatment.

GO–Rg3 loaded with DOX affects contractile machinery, induces cell death, and inflammatory responses

Doxorubicin is widely used to treat HCC (Park et al. 2006; Yeo et al. 2005). To further investigate the GO–Rg3 drug carrier, we performed RNA-seq analysis of GO–Rg3 loaded with DOX and treated Huh7 cells and used untreated cells as a comparison (Fig. 6a). The heat map of the GO–Rg3–DOX-treated group compared with the control group showed that 2619 genes were upregulated, and 2972 genes were downregulated by GO–Rg3–DOX (Fig. 6c). The ECM–receptor interaction, lysosome, cell adhesion molecule, and drug metabolism gene sets were positively enriched, whereas the Wnt signaling, cell cycle, and cellular senescence gene sets were negatively enriched (Fig. 6b).

In Fig. S4a, we show the upregulation of the ACTA1 (actin alpha 1) gene as well as the enrichment of genes with biological functions in actin-mediated cell contraction, actin filament base movement, muscle contraction, and related genes with cellular compartment actin filaments in response to GO–Rg3–DOX compared to the control. Actin acts as the backbone of numerous cellular processes, including cell morphology, cellular and organelle migration, nuclear and cellular division, and muscle contraction. Upadhyay et al. (2021) reviewed the contractile machinery and factors associated with DOX toxicity in patients receiving chemotherapy (Upadhyay et al. 2021). Previous studies have shown that doxorubicin disrupts actin polymerization, leading to stress-fiber

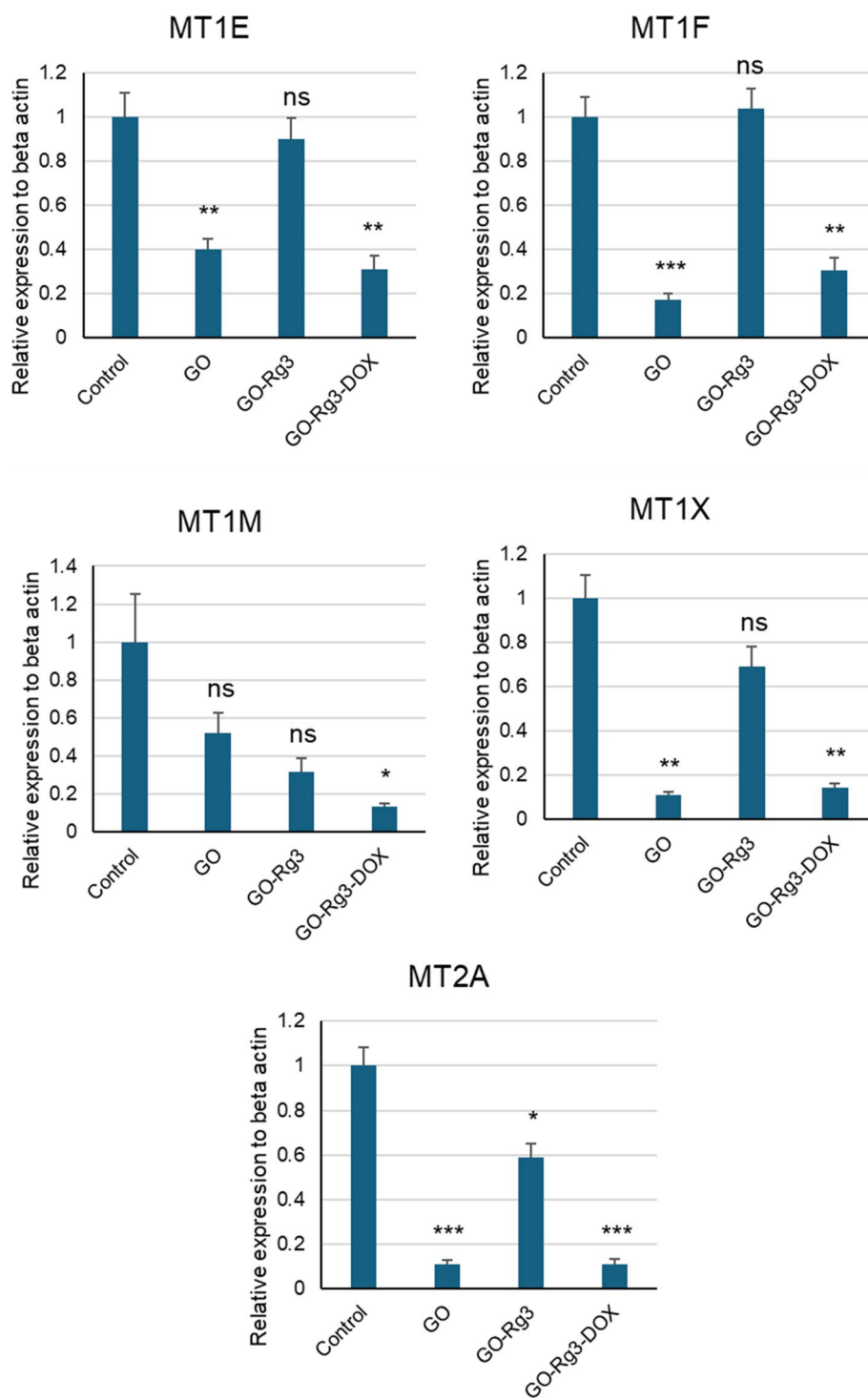


Fig. 5 Validation of RNAseq results of cellular metal-ion related gene responses to GO and GO-Rg3 in Huh7 cells using qPCR analysis. Data are the mean \pm SE of three independent replicates, analyzed using Student's *t* test. ns, not significant; **P* < 0.05; ***P* < 0.01; ****P* < 0.001

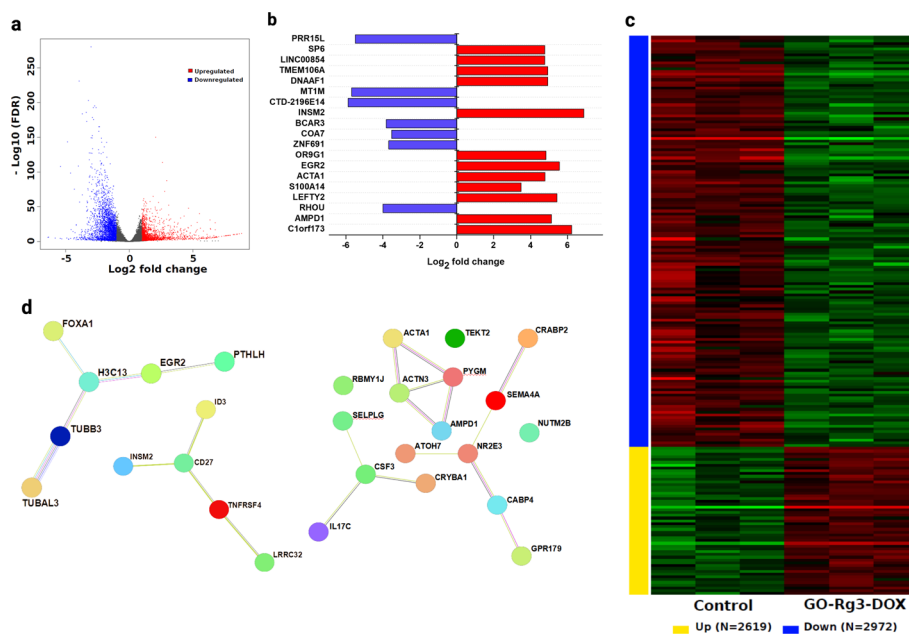


Fig. 6 Transcriptomic analysis comparing the GO-Rg3-DOX and untreated control groups. **a** Volcano plot showing significant downregulated (blue) and elevated (red) DEGs. **b** Bar graph showing \log_2 fold change values for highly expressed significant DEGs. **c** Heat map comparison of total gene expression in the GO-Rg3-DOX and untreated control groups. **d** Network analysis showing functional links between the significant DEGs. DEGs were defined as an adjusted p -value (Benjamini-Hochberg analysis) of less than 0.05 and $|\log_2\text{FC}| > 2$

disorganization, cortical actin ring formation, and changes in cellular adhesion and morphology—both in cytoplasmic and nuclear actin networks (Fourre et al. 2008; Pfitzer et al. 2019; Wei et al. 2015). In addition, DOX hindered actin synthesis at both the transcriptional and translational levels by decreasing mRNA abundance and myofilament loss in rat heart (van der Zanden et al. 2021).

When we compared GO-Rg3-DOX- and GO-treated cells (Fig. 7a), we found that 3116 genes were upregulated, and 2059 genes were downregulated by GO-Rg3-DOX compared with GO (Fig. 7e). The ribosome and oxidative phosphorylation genes that were downregulated by GO (Fig. 2f) were upregulated by GO-Rg3-DOX compared to GO (Fig. S5). Furthermore, the top DEGs with biological functions related to cell death identified in the GO-Rg3-DOX group but not in the GO group included PTGER3, RASSF2, COMP, PAX4, LHX3, PPARGC1A, CXCR4, IRF5, HEY2, IL6, PAK6, ACTA1, ITGB2, PF4, AZU1, EGR3, DIO3, and DLL1 (Fig. 7d). As shown in Fig. 7b, AZU1, EGR3, DLL1, PF4, CXCR4, and PTGER3 were upregulated, and PPARGC1A was downregulated by GO-Rg3-DOX compared to GO. In addition, DEGs with biological functions related to the positive regulation of the tumor necrosis factor superfamily cytokine production (IL17F, CCR2, IL6, PF4, and AZU1) were identified. Gene ontology analysis (Cellular Component and Molecular Function) of the GO-Rg3-DOX treatment group compared to the GO-treated group identified the top DEGs related to chromatin, protein-DNA complex, chromosome, transcription regulator complex compartments, and the top DEGs with molecular functions in DNA-binding transcriptional activator activity, RNA polymerase II cis-regulatory region sequence-specific, transcription regulator

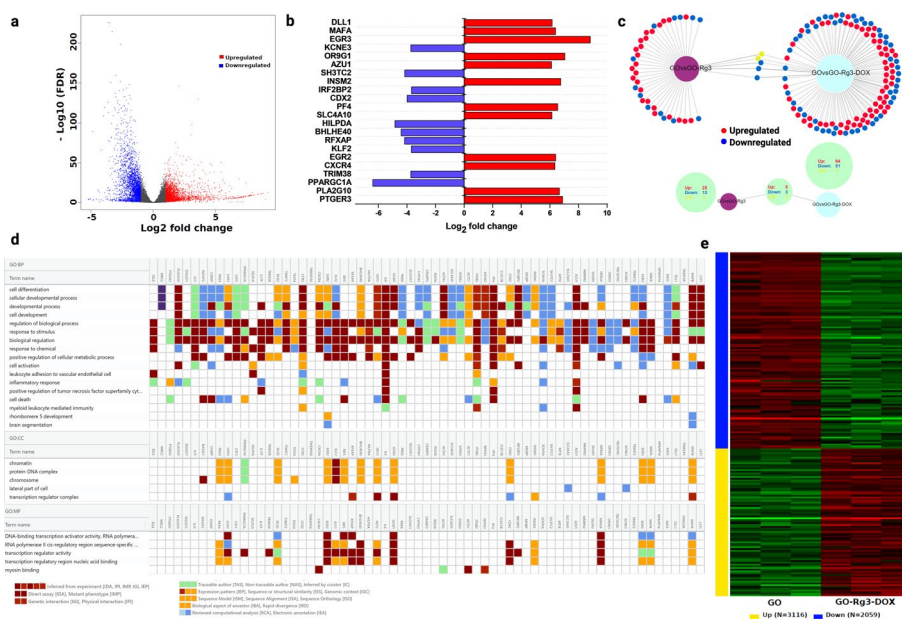


Fig. 7 Transcriptomic analysis comparing the GO and GO-Rg3-DOX groups. **a** Volcano plot depicting substantial down (blue) and upregulated (red) DEGs. **b** Bar graph depicting the log₂ fold change values for significant DEGs with high expression. **c** Network analysis showing up and downregulated genes from the RO and GO-Rg3-DOX groups, revealing unique and commonly shared DEGs. **d** Important biological processes, cellular components, and molecular activities of DEGs, revealed by a Gene Ontology analysis. **e** Heat map depicting total gene expression of the GO and GO-Rg3-DOX groups. DEGs were defined as an adjusted p -value (Benjamini-Hochberg analysis) of less than 0.05 and $|\log_2FC| > 2$. In Gene Ontology experiment, an adjusted p -value (Benjamini-Hochberg analysis) of less than 0.05 was used to detect significant enrichment

activity, and transcription regulatory region nucleic acid binding. In fact, the classical mechanism of action of DOX is to inhibit topoisomerase II, wherein DOX intercalates into DNA, inhibiting the topoisomerase II catalytic step that re-ligates the broken DNA strand after the initial DNA break induction by the enzyme. This ultimately results in enzyme-mediated DNA damage in the form of a double-strand break, which activates DNA damage response and TP53 pathways, leading to cell cycle arrest and cell death (van der Zanden et al. 2021).

Overall, in comparison to GO, the cell response to GO-Rg3-DOX elicits DEGs involved in cell death and transcription regulation, and negative enrichment of cell cycle, which coincided with the reduced viability of GO-Rg3-DOX-treated Huh cells (Rahimi et al. 2023). This suggests the potential role of DOX in cell cycle arrest and cell death. The effect of GO-Rg3-DOX on reduced viability of human breast cancer MDA-MB-231 cells was also previously assessed by our group.

We further validated the RNA-Seq data on cell cycle pathway genes using qPCR. In fact, there was no significant difference in the expression of cell cycle pathway genes, such as CDC6, BUB1B, and TTK by GO treatment compared to that in the control. Additionally, Wnt signaling pathway genes, such as DKK1, FRAT2, FZD4, and S1AH1, were also evaluated after GO treatment. This result indicated that DKK1 was significantly downregulated, whereas other genes, such as FRAT2, FZD4, and S1AH1, showed no significant differences, and their expression patterns were similar to those of the control, suggesting that GO treatment did not contribute to the inhibition of

the cell cycle pathway. Interestingly, when cells were treated with GO-Rg3-DOX, approximately half of the genes involved in the cell cycle (CDC6 and TTK) and Wnt signaling pathways (DKK1 and FRAT2) were significantly downregulated, indicating that GO-Rg3-DOX significantly contributed to Huh7 cell death (Fig. 8).

In the case of the inflammatory response to GO-Rg3-DOX, we found that genes with molecular functions in cytokine activity were differentially expressed by GO-Rg3-DOX compared with the control (Fig. S4a). Moreover, the top DEGs (SELE, PTGER3, PLA2G10, SIGLEC1, IL17F, CCR2, CXCR4, IRF5, IL6, ITGB2, PF4, SCN11A, and AZU1) involved in the inflammatory response were associated with the GO-Rg3-DOX-treated group compared to the GO-treated group (Fig. 7d). Furthermore, genes with molecular functions in cytokine receptor binding (IL11, PYCARD, IL17F, IL6, LEFTY2, PPBP, and PF4) were differentially expressed in response to GO-Rg3-DOX compared with GO-Rg3 (Fig. S5).

Indeed, numerous studies have demonstrated the favorable biocompatibility of tumor-targeted graphene oxide (GO)-based nanocarriers, such as those conjugated with polyethylene glycol (PEG), folic acid, or peptides (Perini et al. 2021; Shang et al. 2014; Swidan et al. 2023). In comparison, our GO-Rg3-DOX system leverages the natural anti-inflammatory and antioxidant properties of ginsenoside Rg3, which may offer distinct advantages over synthetic targeting ligands. Importantly, our findings showed that GO-Rg3 did not significantly change the expression of metallothionein genes, which are stress-inducible markers in response to nanotoxicity and significantly downregulated by GO. This suggests that the Rg3 component may mitigate GO-associated stress responses at the transcriptional level. While direct comparisons are challenging due to differences in model systems and evaluation criteria, our study complements the growing body of work on GO biocompatibility by demonstrating a natural compound-based conjugate that shows both therapeutic synergy and reduced hepatic stress signaling.

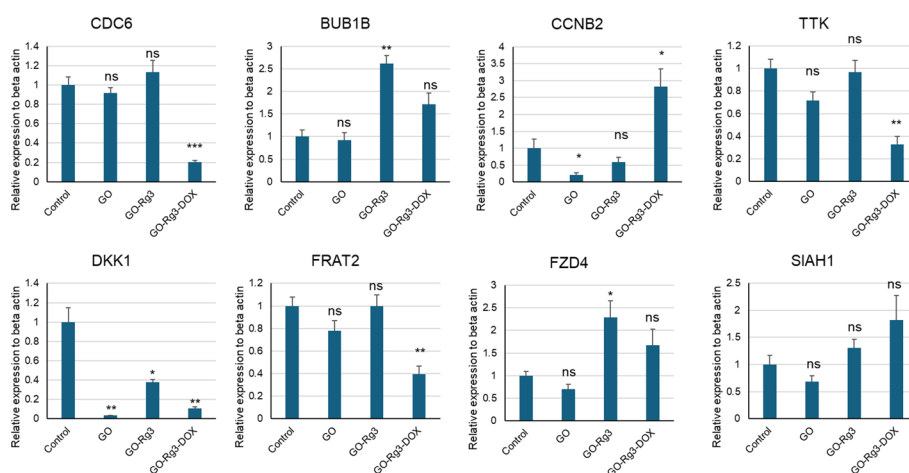


Fig. 8 Validation of RNAseq results of cell cycle and Wnt pathway genes response to GO and GO-Rg3-DOX in Huh7 cells using qPCR analysis. Data are the mean \pm SE of three independent replicates, analyzed using Student's *t* test. ns, not significant; * $P < 0.05$; ** $P < 0.01$; *** $P < 0.001$

Conclusions

The GO–Rg3 treated samples exhibited a slight variance compared to the control samples, proving the biocompatibility of GO–Rg3 compared to GO alone. Furthermore, the downregulation of MT1F and MT1E genes due to GO treatment may be correlated with the enhanced growth of Huh7 cells. The increased proliferation of Huh7 cells, along with HIF-1 signaling gene set enrichment, may be a potential indicator of hypoxia in GO-treated cells. Given the unwanted effects of GO carriers on cell proliferation and angiogenesis, our *in vitro* results suggest limitations in using GO alone as a drug carrier for cancer treatment; further *in vivo* studies are needed to fully evaluate its systemic behavior and suitability.

Indeed, many multifunctional nanomaterials have been developed to achieve combined therapeutic goals. However, our GO–Rg3–DOX conjugate offers a distinctive and practical approach that sets it apart in several important ways, including:

- **Simplified fabrication process:** The synthesis of GO–Rg3–DOX is based on straightforward conjugation steps, avoiding the need for complex chemical modifications or expensive crosslinkers in previous studies (Hazhir et al. 2019; Zainal-Abidin et al. 2020). This simplicity enhances reproducibility and scalability for future applications.
- **Cost-effective components:** Both graphene oxide and ginsenoside Rg3 are commercially available and relatively inexpensive compared to other high-end synthetic carriers or targeting ligands, reducing the overall cost of nanomaterial production.
- **Dual functionality achieved through natural product Rg3:** The use of Rg3 not only modulates the toxicity profile of GO, but also imparts intrinsic therapeutic properties (anti-inflammatory, anti-metastatic, hepatoprotective) (Zhou et al. 2018) making

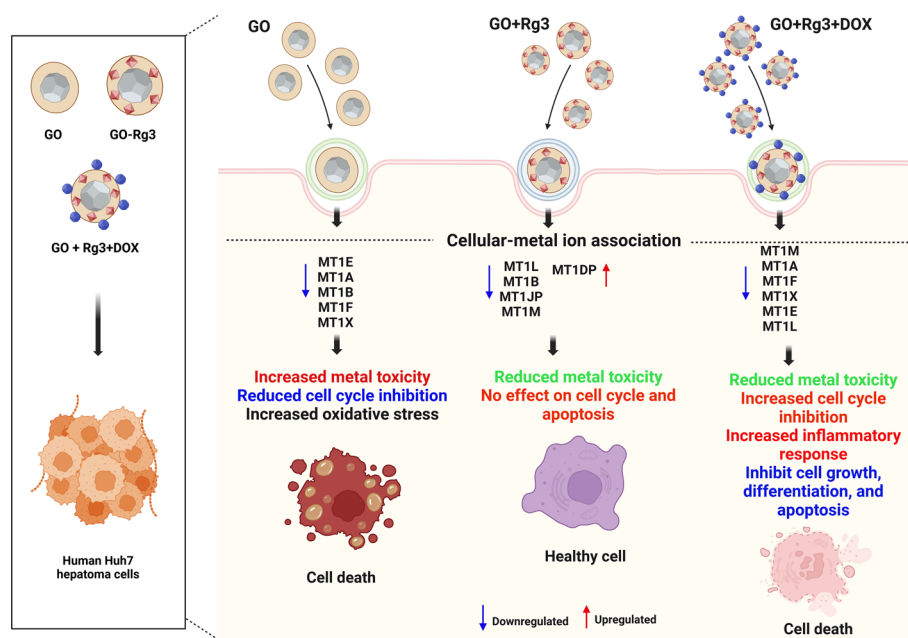


Fig. 9 Schematic representation of the cellular responses to GO alone, GO–Rg3, and GO–Rg3–DOX in hepatocarcinoma cells

it a truly synergistic component rather than an inert stabilizer or passive carrier. This design avoids the need to separately introduce multiple functional agents.

- **Biocompatibility advantage:** In contrast to more synthetically elaborate carriers, GO–Rg3–DOX exhibits improved biocompatibility, as supported by no significant expression of metallothionein genes and reduced cytotoxicity by GO–Rg3.
- **Practical relevance over theoretical sophistication:** While other systems may incorporate more features, they often suffer from increased complexity, potential immunogenicity, and difficulty in clinical translation. Our system focuses on therapeutically relevant, feasible improvements with minimal material complexity.

Toxicological studies on GO revealed that iron deficiency in eukaryotes and prokaryotes is caused by binding to the O-functional groups of GO, which sequester iron and disrupt iron-related physiological and metabolic processes [32]. Thus, one reason behind our results regarding the top DEGs involved in the cellular response to cadmium ions, stress response to metal ions, cellular response to metal ions, transition metal ion binding, ion binding, and downregulation of MT genes could be the disruption of iron physiological and metabolic processes (Fig. 9) However, this needs to be further verified by measuring the intra- and extracellular iron concentrations in future studies.

Supplementary Information

The online version contains supplementary material available at <https://doi.org/10.1186/s12645-025-00345-y>.

Additional file 1 (Fig. S1. Transcriptomic analysis comparing the GO and untreated control groups. (a) Network analysis of substantial DEGs revealed functional relationships between the genes. (b) Gene set enrichment analysis performed for selective pathways associated with DEGs. DEGs were defined as an adjusted p-value (Benjamini–Hochberg analysis) of less than 0.05 and $|\log_2FC| > 2$. In gene ontology and GSEA experiments, an adjusted p-value (Benjamini–Hochberg analysis) of less than 0.05 was used to detect significant enrichment.)

Additional file 2 (Fig. S2. Comparing the transcriptomes changes of GO–Rg3 with untreated control groups. (a) A volcano plot shows important downregulated (blue) and upregulated (red) DEGs. (b) A bar graph with \log_2 fold change values based on highly expressed significant DEGs. (c) Network analysis of DEGs. (d) Total gene expression displayed in a heat map comparison between the GO–Rg3 and untreated control group. (e) The biological process, cellular component, and molecular function of important DEGs were revealed by gene ontology analysis. (f) Gene set enrichment analysis carried out for particular pathways connected to the DEGs. (g) Pathway network analysis of spliceosome-associated genes. DEGs were defined as an adjusted p-value (Benjamini–Hochberg analysis) of less than 0.05 and $|\log_2FC| > 2$. In gene ontology and GSEA experiments, an adjusted p-value (Benjamini–Hochberg analysis) of less than 0.05 was used to detect significant enrichment.)

Additional file 3 (Fig. S3. Transcriptomic analysis comparing the GO and GO–Rg3 groups. (a) Gene set enrichment analysis of particular pathways that correlate with DEG genes. (b) Gene ontology analysis was carried out for significant DEGs. DEGs were defined as an adjusted p-value (Benjamini–Hochberg analysis) of less than 0.05 and $|\log_2FC| > 2$. In gene ontology and GSEA experiments, an adjusted p-value (Benjamini–Hochberg analysis) of less than 0.05 was used to detect significant enrichment.)

Additional file 4 (Fig. S4. Transcriptomic analysis comparing the GO–Rg3–DOX and untreated control groups. (a) Gene ontology study showing important DEG biological processes, cellular components, and molecular functions. (b) Gene set enrichment analysis was performed on specific pathways corresponding to DEGs. DEGs were defined as an adjusted p-value (Benjamini–Hochberg analysis) of less than 0.05 and $|\log_2FC| > 2$. In gene ontology and GSEA experiments, an adjusted p-value (Benjamini–Hochberg analysis) of less than 0.05 was used to detect significant enrichment.)

Additional file 5 (Fig. S5. Transcriptomic analysis comparing the GO and GO–Rg3–DOX groups. Gene set enrichment analysis of distinct pathways associated with DEGs. DEGs were defined as an adjusted p-value (Benjamini–Hochberg analysis) of less than 0.05 and $|\log_2FC| > 2$. In gene ontology and GSEA experiments, an adjusted p-value (Benjamini–Hochberg analysis) of less than 0.05 was used to detect significant enrichment.)

Additional file 6.

Author contributions

Sri Renukadevi Balusamy: writing—original draft, formal analysis, data curation. Shadi Rahimi: writing—original draft, formal analysis, data curation. Olena Tkachova: formal analysis, data curation. Seungah Lee: methodology, formal analysis, Suresh Ramakrishna: funding acquisition, visualization, validation, Ivan Mijakovic: supervision, project

administration, investigation, Haribalan Perumalsamy: methodology, funding acquisition, formal analysis, data curation, conceptualization.

Funding

Open access funding provided by Chalmers University of Technology. This work was supported by the National Research Foundation of Korea (NRF) grant funded by the Korean Government (MSIT) (No. 2023R1A2C2002623, No. RS-2024-00341469).

Data availability

Raw RNA sequencing data and raw read counts are accessible through the GEO Series accession number GSE185139 (<https://www.ncbi.nlm.nih.gov/geo/query/acc.cgi?acc=GSE185139>).

Declarations

Ethics approval and consent to participate

Not applicable.

Consent for publication

Not applicable.

Competing interests

The authors declare no competing interests.

Author details

¹Department of Food Science and Biotechnology, Sejong University, Gwangjin-gu, Seoul, Republic of Korea. ²Systems and Synthetic Biology Division, Department of Life Sciences, Chalmers University of Technology, SE-412 96 Gothenburg, Sweden. ³Department of Applied Chemistry and Institute of Natural Sciences, Kyung Hee University, Yongin-si, Gyeonggi-do 17104, Republic of Korea. ⁴Graduate School of Biomedical Science and Engineering, Hanyang University, Seoul 04763, Republic of Korea. ⁵College of Medicine, Hanyang University, Seoul 04763, South Korea. ⁶The Novo Nordisk Foundation, Center for Biosustainability, Technical University of Denmark, 2800 Kongens Lyngby, Denmark. ⁷Research Institute for Convergence of Basic Science, Hanyang University, Seoul 04763, South Korea. ⁸Center for Creative Convergence Education, Hanyang University, Seoul, Republic of Korea.

Received: 9 April 2025 Revised: 22 July 2025 Accepted: 6 September 2025

Published online: 04 October 2025

References

- Cao Y, Ye Q, Zhuang M, Xie S, Zhong R, Cui J et al (2017) Ginsenoside Rg3 inhibits angiogenesis in a rat model of endometriosis through the VEGFR-2-mediated PI3K/Akt/mTOR signaling pathway. *PLoS ONE* 12(11):e0186520
- Chen Y-S, Yanagida F, Shinohara T (2005) Isolation and identification of lactic acid bacteria from soil using an enrichment procedure. *Lett Appl Microbiol* 40(3):195–200
- Demidenko R, Daniunaite K, Bakavicius A, Sabaliauskaite R, Skeberdyte A, Petroska D et al (2017) Decreased expression of MT1E is a potential biomarker of prostate cancer progression. *Oncotarget* 8(37):61709
- Fourre N, Millerot-Serruot E, Garnotel R, Zahm J, Bonnet N, Millot J et al (2008) Extracellular matrix proteins protect human HT1080 cells against the antimigratory effect of doxorubicin. *Cancer Sci* 99(8):1699–1705
- Guo C, Book-Newell B, Irudayaraj J (2011) Protein-directed reduction of graphene oxide and intracellular imaging. *Chem Commun* 47(47):12658–12660
- Guo Y, Xiao Z, Yang L, Gao Y, Zhu Q, Hu L et al (2020) Hypoxia-inducible factors in hepatocellular carcinoma (review). *Oncol Rep* 43(1):3–15
- Hazhir N, Chekin F, Raouf JB, Fathi Sh (2019) A porous reduced graphene oxide/chitosan-based nanocarrier as a delivery system of doxorubicin. *RSC Adv* 9(53):30729–30735
- Hu S, Zhu Y, Xia X, Xu X, Chen F, Miao X et al (2019) Ginsenoside Rg3 Prolongs Survival of the Orthotopic Hepatocellular Carcinoma Model by Inducing Apoptosis and Inhibiting Angiogenesis. *Anal Cell Pathol* 2019(1):3815786
- Jiang C, Zhao H, Xiao H, Wang Y, Liu L, Chen H et al (2021) Recent advances in graphene-family nanomaterials for effective drug delivery and phototherapy. *Expert Opin Drug Deliv* 18(1):119–138
- Johnson DE, O'Keefe RA, Grandis JR (2018) Targeting the IL-6/JAK/STAT3 signalling axis in cancer. *Nat Rev Clin Oncol* 15(4):234–248
- Lammel T, Boisseaux P, Fernández-Cruz M-L, Navas JM (2013) Internalization and cytotoxicity of graphene oxide and carboxyl graphene nanoplatelets in the human hepatocellular carcinoma cell line Hep G2. *Part Fibre Toxicol* 10(1):27
- Li Y, Liu Y, Fu Y, Wei T, Le Guyader L, Gao G et al (2012) The triggering of apoptosis in macrophages by pristine graphene through the MAPK and TGF-beta signaling pathways. *Biomaterials* 33(2):402–411
- Liu Q, Lu F, Chen Z (2020) Identification of MT1E as a novel tumor suppressor in hepatocellular carcinoma. *Pathol Res Pract* 216(11):153213
- Lu D-D, Chen Y-C, Zhang X-R, Cao X-R, Jiang H-Y, Yao L (2003) The relationship between metallothionein-1F (MT1F) gene and hepatocellular carcinoma. *Yale J Biol Med* 76(2):55–62
- Majumder S, Roy S, Kaffenberger T, Wang B, Costinean S, Frankel W et al (2010) Retracted: loss of Metallothionein predisposes mice to Diethylnitrosamine-induced hepatocarcinogenesis by activating NF-κB target genes. *Cancer Res* 70(24):10265–10276

- McKeown SR (2014) Defining normoxia, physoxia and hypoxia in tumours—implications for treatment response. *Br J Radiol* 87(1035):20130676
- Moffatt P, Séguin C (1998) Expression of the Gene Encoding Metallothionein-3 in Organs of the Reproductive System. *DNA Cell Biol* 17(6):501–510
- Mukherjee S, Sriram P, Barui AK, Nethi SK, Veeriah V, Chatterjee S et al (2015) Graphene oxides show angiogenic properties. *Adv Healthc Mater* 4(11):1722–1732
- Nakhjavani M, Smith E, Townsend AR, Price TJ, Hardingham JE (2020) Anti-angiogenic properties of ginsenoside Rg3. *Molecules* 25(21):4905
- Park Y, Yu E (2013) Expression of metallothionein-1 and metallothionein-2 as a prognostic marker in hepatocellular carcinoma. *J Gastroenterol Hepatol* 28(9):1565–1572
- Park SH, Lee Y, Han SH, Kwon SY, Kwon OS, Kim SS et al (2006) Systemic chemotherapy with doxorubicin, cisplatin and capecitabine for metastatic hepatocellular carcinoma. *BMC Cancer* 6(1):3
- Peng C, Hu W, Zhou Y, Fan C, Huang Q (2010) Intracellular imaging with a graphene-based fluorescent probe. *Small* 6(15):1686–1692
- Perini G, Palmieri V, Ciasca G, Primiano A, Gervasoni J, De Spirito M et al (2021) Functionalized graphene quantum dots modulate malignancy of glioblastoma multiforme by downregulating neurospheres formation. *C (Basel)* 7(1):4
- Pfitzer L, Moser C, Gegenfurtner F, Arner A, Foerster F, Atzberger C et al (2019) Targeting actin inhibits repair of doxorubicin-induced DNA damage: a novel therapeutic approach for combination therapy. *Cell Death Dis* 10(4):302
- Qu Y, He F, Yu C, Liang X, Liang D, Ma L et al (2018) Advances on graphene-based nanomaterials for biomedical applications. *Mater Sci Eng C Mater Biol Appl* 90:764–780
- Rahimi S, Chen Y, Zareian M, Pandit S, Mijakovic I (2022) Cellular and subcellular interactions of graphene-based materials with cancerous and non-cancerous cells. *Adv Drug Deliv Rev* 189:114467
- Rahimi S, van Leeuwen D, Roshanzamir F, Pandit S, Shi L, Sasanian N et al (2023) Ginsenoside Rg3 reduces the toxicity of Graphene oxide used for pH-responsive delivery of doxorubicin to liver and breast cancer cells. *Pharmaceutics* 15:391
- Roesijadi G (1996) Metallothionein and its role in toxic metal regulation. *Comp Biochem Physiol C Pharmacol Toxicol Endocrinol* 113(2):117–123
- Ryu H-H, Jung S, Jung T-Y, Moon K-S, Kim I-Y, Jeong Y-I et al (2012) Role of metallothionein 1E in the migration and invasion of human glioma cell lines. *Int J Oncol* 41(4):1305–1313
- Shang W, Zhang X, Zhang M, Fan Z, Sun Y, Han M et al (2014) The uptake mechanism and biocompatibility of graphene quantum dots with human neural stem cells. *Nanoscale* 6(11):5799–5806
- Si M, Lang J (2018) The roles of metallothioneins in carcinogenesis. *J Hematol Oncol* 11(1):107
- Sutherland DEK, Stillman MJ (2014) Challenging conventional wisdom: single domain metallothioneins. *Metallomics* 6(4):702–728
- Swidan MM, Essa BM, Sakr TM (2023) Pristine/folate-functionalized graphene oxide as two intrinsically radioiodinated nanotheranostics: self/dual in vivo targeting comparative study. *Cancer Nanotechnol* 14(1):6
- Szmidt M, Stankiewicz A, Urbańska K, Jaworski S, Kutwin M, Wierzbicki M et al (2019) Graphene oxide down-regulates genes of the oxidative phosphorylation complexes in a glioblastoma. *BMC Mol Biol* 20(1):2
- Tang Y-C, Zhang Y, Zhou J, Zhi Q, Wu M-Y, Gong F-R et al (2018) Ginsenoside Rg3 targets cancer stem cells and tumor angiogenesis to inhibit colorectal cancer progression in vivo. *Int J Oncol* 52(1):127–138
- Upadhyay S, Gupta KB, Mantha AK, Dhiman M (2021) A short review: doxorubicin and its effect on cardiac proteins. *J Cell Biochem* 122(2):153–165
- van der Zanden SY, Qiao X, Neefjes J (2021) New insights into the activities and toxicities of the old anticancer drug doxorubicin. *FEBS J* 288(21):6095–6111
- Wang Z, Huang P, Bhirde A, Jin A, Ma Y, Niu G et al (2012) A nanoscale graphene oxide-peptide biosensor for real-time specific biomarker detection on the cell surface. *Chem Commun* 48(78):9768–9770
- Wang W, Li K, Xiao W (2024) The pharmacological role of Ginsenoside Rg3 in liver diseases: a review on molecular mechanisms. *J Ginseng Res* 48(2):129–139
- Wei L, Surma M, Gough G, Shi S, Lambert-Cheatham N, Chang J et al (2015) Dissecting the mechanisms of doxorubicin and oxidative stress-induced cytotoxicity: the involvement of actin cytoskeleton and ROCK1. *PLoS ONE* 10(7):e0131763
- Yang X, Wang Y, Huang X, Ma Y, Huang Y, Yang R et al (2011) Multi-functionalized graphene oxide based anticancer drug-carrier with dual-targeting function and pH-sensitivity. *J Mater Chem* 21(10):3448–3454
- Yang R, Roshani D, Gao B, Li P, Shang N (2024) Metallothionein: a comprehensive review of its classification, structure, biological functions, and applications. *Antioxidants (Basel)*. 13(7):825
- Yeo W, Mok TS, Zee B, Leung TWT, Lai PBS, Lau WY et al (2005) A randomized phase III study of doxorubicin versus cisplatin/interferon α -2b/doxorubicin/fluorouracil (PIAF) combination chemotherapy for unresectable hepatocellular carcinoma. *JNCI J Natl Cancer Inst* 97(20):1532–1538
- Yue PYK, Wong DYL, Wu PK, Leung PY, Mak NK, Yeung HW et al (2006) The angiostatic effects of 20(R)- ginsenoside Rg3. *Biochem Pharmacol* 72(4):437–445
- Zainal-Abidin MH, Hayyan M, Ngho GC, Wong WF (2020) Doxorubicin loading on functional graphene as a promising nanocarrier using ternary deep eutectic solvent systems. *ACS Omega* 5(3):1656–1668
- Zhang Q, Wu Z, Li N, Pu Y, Wang B, Zhang T et al (2017) Advanced review of graphene-based nanomaterials in drug delivery systems: synthesis, modification, toxicity and application. *Mater Sci Eng C, Mater Biol Appl* 77:1363–1375
- Zhou T, Zhang B, Wei P, Du Y, Zhou H, Yu M et al (2014) Energy metabolism analysis reveals the mechanism of inhibition of breast cancer cell metastasis by PEG-modified graphene oxide nanosheets. *Biomaterials* 35(37):9833–9843
- Zhou Y, Hou J, Liu W, Ren S, Wang Y, Zhang R et al (2018) 20(R)-ginsenoside Rg3, a rare saponin from red ginseng, ameliorates acetaminophen-induced hepatotoxicity by suppressing PI3K/AKT pathway-mediated inflammation and apoptosis. *Int Immunopharmacol* 59:21–30
- Zhu J, Li B, Xu M, Liu R, Xia T, Zhang Z et al (2020) Graphene Oxide Promotes Cancer Metastasis through Associating with Plasma Membrane To Promote TGF- β Signaling-Dependent Epithelial-Mesenchymal Transition. *ACS Nano* 14(1):818–827

Publisher's Note

Springer Nature remains neutral with regard to jurisdictional claims in published maps and institutional affiliations.